# Nanoscale

Check for updates

# 2D MoS₂ nanosheets on 1D anodic TiO₂ nanotube layers: an efficient co-catalyst for liquid and gas phase photocatalysis†

Martin Motola, [a] Michal Baudys, [b] Raul Zazpe, [a,c] Miloš Krbal, [a]
Jan Michalička, [c] Jhonatan Rodriguez-Pereira, [a] David Pavliňák, [d] Jan Přikryl, [a]
Luděk Hromádko, [a,c] Hanna Sopha, [a,c] Josef Krýsa [b] and Jan M. Macak *[a,c]

One-dimensional TiO₂ nanotube layers with different dimensions were homogeneously decorated with 2D MoS₂ nanosheets *via* atomic layer deposition and employed for liquid and gas phase photocatalysis. The 2D MoS₂ nanosheets revealed a high amount of exposed active edge sites and strongly enhanced the photo-catalytic performance of TiO₂ nanotube layers.

Self-organized TiO₂ nanotube (TNT) layers, prepared *via* electrochemical anodization,[1–3] represent unique one-dimensional (1D) nanomaterials. TNT layers are commonly accepted to be excellent for photoelectrochemical applications, in particular photocatalysis.[1–4] Their unique geometry and properties, such as a high surface area, tunability of dimensions, and strong light absorption, are their main advantages over other TiO₂ nanostructures.[5–9] The photocatalysis on TiO₂ surfaces is based on UV light absorption, generation of e⁻/h⁺ pairs, and formation of radicals with high oxidizing power that subsequently decompose organic matter.[4,5] Due to the band gap of ~3.2 eV for anatase TiO₂, a photoresponse can only be generated by UV light irradiation.[10–12]

In recent years, 2D transition metal dichalcogenides, especially MoS₂, have attracted considerable attention owing to their suitable band gap for VIS light absorption, high carrier mobility and relatively good stability against photocorrosion.[13,14] Structurally, MoS₂ is composed of covalently bound S–Mo–S

stacks held together by weak van der Waals interactions determining the 2D nature of the crystalline phases.[15] Bulk MoS₂ has an indirect band gap of ~1.3 eV which increases, due to quantum confinement effects, to ~1.9 eV for monolayer sheets.[16,17] Approximately 25% of edge sites are active for the photocatalytic reaction.[18] All in all, mono- and few-layered sheets of MoS₂ exhibit a range of intriguing properties, absent in the bulk.

The intimate contact between TiO₂ and MoS₂ results into a type-II heterojunction structure with favorable positions of conduction and valence bands in the energy diagram.[13] The photogenerated e⁻ from the valence band of MoS₂ are directly transferred to its conduction band, leaving the newly created h⁺ in the valence band of MoS₂. As the conduction band potential of TiO₂ is lower compared to that of MoS₂, TiO₂ acts as an electron acceptor of the photogenerated e⁻ from the conduction band of MoS₂.[19] Moreover, the e⁻ are trapped by oxygen molecules in the aqueous solution to form singlet oxygen.[20] Simultaneously, the photogenerated h⁺ are captured within MoS₂, effectively suppressing the recombination rate of charge carriers, thus improving the photocatalytic activity.[21] The h⁺ reacts with either H₂O or OH⁻ adsorbed onto the TiO₂ surface to produce ˙OH, and the e⁻ react with O₂ to form ˙O₂⁻.[22] Consequently, both ˙OH and ˙O₂⁻ radicals decompose various organic pollutants to CO₂ and H₂O.[22]

So far, many methods have been explored to decorate TiO₂ materials by MoS₂, such as sputtering,[16] hydrothermal,[23,24] photoassisted electrodeposition,[24] solvothermal,[25] sol–gel,[26,27] chemical vapor deposition,[28] exfoliation,[29,30] photocatalytic reduction of (NH₄)₂MoS₄ to MoS₂,[31] and liquid ultrasonic mixing.[32] However, none of the above-mentioned techniques is suitable for the decoration of 1D TNT layers, as only very inhomogeneous decoration by MoS₂ nanosheets of these layers throughout their volume can be achieved. Atomic layer deposition (ALD) is the most suitable method for homogeneous decoration and coating of various 1D nanomaterials, including TNTs.[33,34] ALD is based on sequential self-limited adsorption of vapors of compatible precursors on surfaces which allows conformity all over the surface with controllable thickness at the atomic level.[33]

*ᵃCenter of Materials and Nanotechnologies, Faculty of Chemical Technology, University of Pardubice, Nam. Cs. Legii 565, 53002 Pardubice, Czech Republic. E-mail: jan.macak@upce.cz*
*ᵇDepartment of Inorganic Technology, University of Chemistry and Technology Prague, Technicka 5, 16628 Prague, Czech Republic*
*ᶜCentral European Institute of Technology, Brno University of Technology, Purkynova 123, 61200 Brno, Czech Republic*
*ᵈDepartment of Physical Electronics, Masaryk University, Kotlarska 2, 61137 Brno, Czech Republic*

2D $MoS_2$ nanosheets grown on wider band gap semi-conductors (e.g. $TiO_2$) serve as a sensitizer and enable enhanced production of hydrogen[16,35–37] and photodegradation of organic pollutants.[38,39] Although the photocatalysis of $MoS_2$ decorated TNT layers is reported,[16,24,31,40–42] all publications show inhomogeneous decoration of TNT layers with thickness >1 μm. Only TNT layers with thickness <1 μm were homogeneously decorated.[31,40,42] Furthermore, these publications focus mainly on hydrogen evolution. Only a few publications focus on the photodegradation of pollutants,[24,41,43,44] however, solely in the liquid phase. No publications focus on the photocatalytic activity of these layers in the gas phase.

In the present work, liquid (i.e. using a model organic dye) and gas phase (i.e. hexane-to-$CO_2$ conversion) photocatalyses are reported for TNT layers homogenously decorated by $MoS_2$ nanosheets. ALD was used for the homogeneous decoration of TNT layers with different dimensions using a recently described process.[45]

Fig. 1A–D show representative top-view and cross-sectional view scanning electron microscopy (SEM) images of TNT layers. ~5 μm thick TNT layers with an inner tube diameter of ~230 nm on a 2.25 $cm^2$ area were used for liquid phase photocatalysis (Fig. 1A and B). For gas phase photocatalysis (Fig. 1C and D), TNT layers with a thickness of ~1 μm and an inner diameter of ~45 nm on a 50 $cm^2$ area were used. Both types of TNT layers have a very similar aspect ratio of approx. 22. The

reason for using different types of TNT layers for gas phase photocatalysis is two-fold: (i) the available gas phase setup requires the use of 50 $cm^2$ areas, and (ii) technological difficulties in growing 5 μm thick nanotube layers with the same (or at least similar) inner diameter nanotubes, as on the lab scale.[46,47] Details are discussed in the ESI.† Nevertheless, we achieved uniform, well adhering and crack-free TNT layers for both types of samples (ESI, Fig. S1†).

For the purpose of comparison, we used TNT layers with 3 different ALD $MoS_2$ cycles: 1, 2 and 5. After the ALD of $MoS_2$, it was possible to observe $MoS_2$ ultrathin nanosheets on TNT layers only by TEM (not SEM), due to their extremely small dimensions. Fig. 1E shows a representative STEM HAAD image and the corresponding STEM EDX elemental maps of the chemical distribution of Mo and S elements on the fragment of a nanotube wall in the cross-sectional view after 2 $MoS_2$ ALD cycles. This homogeneous decoration of TNT layers with $MoS_2$ nanosheets was revealed over their entire volume. X-ray diffraction (XRD), micro-Raman spectroscopy (mRS) and X-ray photoelectron spectroscopy (XPS) were carried out to obtain additional information on the crystalline structure and composition (all in the ESI†). While XRD measurements could be carried out on TNT layers, mRS and XPS could be, due to the nature of these techniques and optimal signal-to-noise ratio, carried out only on planar Si wafers (ALD decorated in parallel with the TNT layers). The native $SiO_2$ thin layer on the Si wafer was not removed before ALD decoration. From XRD patterns (Fig. S2†), only diffractions of $TiO_2$ anatase and diffractions of Ti from the underlying Ti substrate were identified for blank TNT layers. In all $MoS_2$ decorated TNT layers, additional diffraction of $MoS_2$ at a $2\theta$ of ~14.3° is visible (26622-ICSD).[45] This clearly shows the successful growth of crystalline $MoS_2$ nanosheets during the ALD process. Nevertheless, several peaks are observed stemming from the nonstoichiometric $Mo_XS_Y$ compositions. The presence of $MoS_2$ is further confirmed by mRS (Fig. S3†). Signals at ~384 $cm^{-1}$ and ~403 $cm^{-1}$ which correspond to the $E_{2g}^1$ and $A_{1g}$ modes of $MoS_2$, respectively, are observed (discussed in detail in the ESI†) when decorated by 5c $MoS_2$.[48] The obtained Raman spectra did not show any signal for 1c and 2c $MoS_2$ due to the extremely small dimensions of the nanosheets. Only signals from the underlying substrate were observed. Nevertheless, the presence of $MoS_2$ is confirmed by XPS for all ALD cycles (Fig. S4†). The high resolution spectra of Mo 3d show a doublet with the Mo $3d_{5/2}$ peak at 229.4 eV corresponding to the $Mo^{4+}$ oxidation state and S 2p spectra show a doublet with the S $2p_{3/2}$ peak at 162.2 eV corresponding to the $S^{2-}$ oxidation state. The determined S/Mo ratios are 2.03, 2.13 and 2.31 for 1c, 2c and 5c $MoS_2$, respectively. The doublet shape of Mo 3d is wider compared to that of pure $MoS_2$.[45] This is due to the presence of an additional $Mo^{6+}$ oxidation state in the form of $MoO_3$, which can have a two-fold origin. Either it is the result of a partial oxidation of Mo species following the ALD process or it stems from the reaction with the O species (in the $TiO_2$ and $SiO_2$) present on the interface between substrates and the decorated $MoS_2$ nanosheets. Moreover, the decrease in O 1s peaks
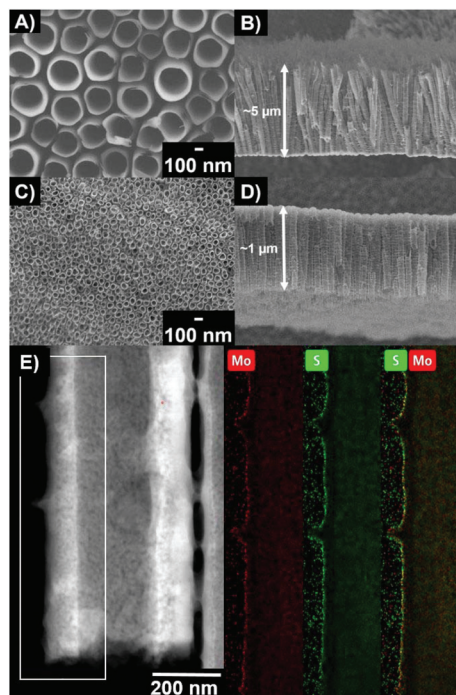


Fig. 1 SEM images of the as-prepared $TiO_2$ nanotube (TNT) layers: (A, C) top-view, and (B, D) cross-sectional view of 5 μm and 1 μm thick TNT layers. (E) STEM HAAD image and the corresponding STEM EDX elemental maps (obtained from the marked region) show the decoration of Mo and S species on the TNT wall and reveal a homogeneous $MoS_2$ decoration along the TNT wall after 2 $MoS_2$ ALD cycles.

reflects the increasing amount of S–Mo–S stacks within nanosheets. The signal intensity follows the order 1 > 2 > 5 $MoS_2$ ALD cycles (from the most intense to less intense).

The photoelectrochemical characteristics were recorded for blank and $MoS_2$ decorated 5 μm thick TNT layers in the wavelength range from 310 nm to 800 nm, as shown in Fig. 2 and the ESI (Fig. S5†). The extension of the photocurrent responses into the visible spectral region relative to the blank TNT layers is observed for all TNT layers decorated with $MoS_2$ nanosheets. Incident photon-to-electron conversion efficiency (IPCE, Fig. 2A) values were doubled for TNT layers with 1 and 2 $MoS_2$ cycles, reaching ∼40%, in comparison with the blank TNT layer in the wavelength range of 350–370 nm. Due to the band gap of $TiO_2$ of ∼3.2 eV there is no response in the VIS spectral region for blank TNT layers. In the wavelength range of

410–430 nm, the IPCE values reached ∼20% for TNT layers with 1 and 2 $MoS_2$ cycles and about ∼10% for TNTs + 5c $MoS_2$. This clearly shows a stronger ability of $MoS_2$ decorated TNT layers to produce charge carriers and more separated e⁻ compared to the blank layers. Also the annihilation of $TiO_2$ surface states by $MoS_2$ nanosheets might come into play, as shown previously.[37] To examine the photoresponse of TNT layers over a range of wavelengths, the photocurrent transients were recorded at a fixed bias of +0.4 V$_{vs. Ag/AgCl}$ with light on/off for 10 s period in the UV (Fig. 2B) and VIS spectral range (Fig. 2C). The $MoS_2$ decorated TNT layers show a good photocurrent switching performance with a fast response time. The type-II heterojunction interface of the $MoS_2$ (with a direct band gap)/ $TiO_2$ heterostructure and also the $TiO_2$ surface state annihilation are responsible for such an enhancement.[4,34,40] In contrast, an increased thickness of $MoS_2$ nanosheets (i.e. theoretically 5 ALD cycles correspond to 5 S–Mo–S stacks with an indirect band gap) decreased the photoresponse in the UV spectral region compared to the blank layers. This is due to the low electron conductivity of $MoS_2$ that limits the e⁻ transfer.[44,49] Moreover, with an increased number of ALD cycles, the increasing number of S–Mo–S stacks could significantly suppress the e⁻ transfer in the direction perpendicular to the basal plane of the $MoS_2$ nanosheets.[49]

Fig. 3A and B show the photocatalytic performance (of the same TNT layers shown in Fig. 2) for the liquid phase photodegradation of methylene blue (MB) under UV and VIS irradiation, respectively. It follows a pseudo-first-order reaction.[2] Thus, its kinetics can be expressed from the linear vari-
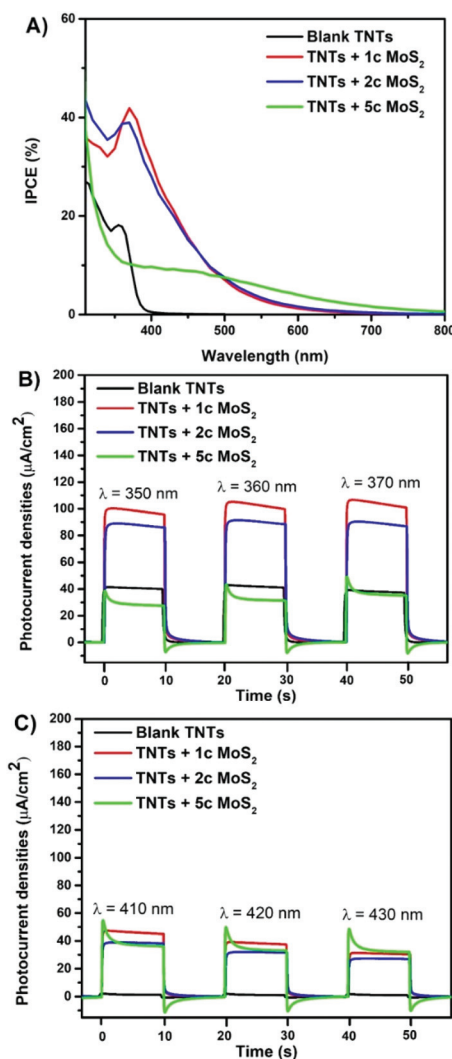


**Fig. 2** (A) Incident photon-to-electron conversion efficiency (IPCE) vs. wavelength. Photocurrent transients recorded at (B) 350 nm, 360 nm, and 370 nm, respectively, and (C) 410 nm, 420 nm, and 430 nm, respectively, for blank, and $MoS_2$ decorated TNT layers. The "Xc" specifies the number of $MoS_2$ ALD cycles. All data recorded in an aqueous 0.1 M $Na_2SO_4$ at 0.4 V$_{vs. Ag/AgCl}$.
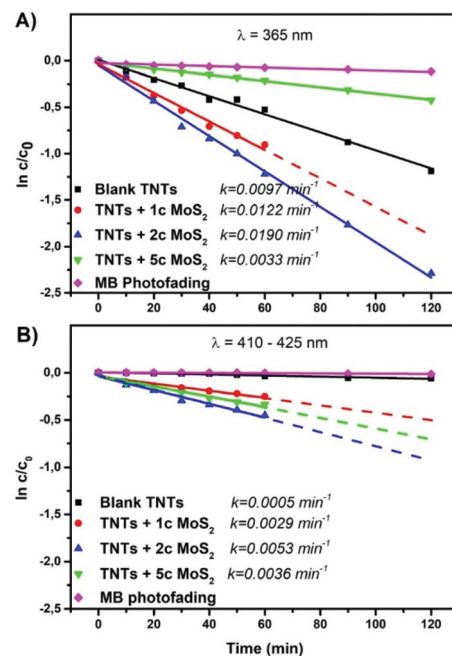


**Fig. 3** Liquid phase photocatalysis: degradation rates of methylene blue (MB) for blank and $MoS_2$ decorated TNT layers and the resulting kinetic rate constants: (A) UV: λ = 365 nm and (B) VIS: λ = 410−425 nm. The "Xc" specifies the number of $MoS_2$ ALD cycles.

ation of $\ln c/c_0$ as a function of time. The resulting kinetic rate constants are shown in Fig. 3.

The results clearly show that the appropriate $MoS_2$ decoration of TNT layers by 1 or 2 ALD cycles of $MoS_2$ enhances the photocatalytic activity of TNT layers. TNT layers decorated with 5 ALD $MoS_2$ cycles possess worse activities compared to the blank and to those with 1 or 2 cycles under UV irradiation (Fig. 3A). The band gap for this thickest $MoS_2$ nanosheet decoration used in here is indirect,[13,50] and it is mainly the excess of $MoS_2$ on the available $TiO_2$ surface that lowers the photocatalytic activity due to a shading effect.[51,52] This means that $MoS_2$ blocks the incident light absorption by $TiO_2$ and reduces its photoexcitation capacity. Indeed, the higher density (and shading) of $MoS_2$ nanosheets within TNT layers + 5c $MoS_2$ compared to that in TNT layers + 2c $MoS_2$ is clearly observed from STEM EDX (ESI, Fig. S6†). Fig. 3B shows the photodegradation of MB under VIS irradiation. Compared to the photodegradation in the UV spectral range, the photocatalytic activity of TNT layers + 5c $MoS_2$ is enhanced and it is higher than that of TNT layers + 1c $MoS_2$. Indeed, in the VIS spectral region, $MoS_2$ is predominantly responsible for photodegradation due to its lower band gap compared to $TiO_2$. Diffuse reflectance UV-VIS spectra and the corresponding Kubelka–Munk curves (ESI, Fig. S7†) were recorded to determine the optical band gap energy of blank and $MoS_2$ decorated TNT layers. Values of ~3.12 eV, ~1.35 eV, and ~1.19 eV for blank TNT layers, TNT layers + 1c $MoS_2$, and TNT layers + 2c $MoS_2$ were determined, respectively. The difference in the band gap energy can be described as follows. One ALD cycle results into one S–Mo–S stack. Therefore, with an increased number of ALD cycles, the number of S–Mo–S stacks also increases. As the band gap energy of $MoS_2$ is strongly influenced by the number of S–Mo–S stacks, it will decrease with an increased number of these stacks. This suggests that the presence of $MoS_2$ on the surface of $TiO_2$ leads to the change in the electronic structure of $TiO_2$. It is apparent that TNT layers decorated by 1 or 2 ALD cycles of $MoS_2$ possess an increased incident light absorption. For the TNT layers + 5c $MoS_2$, it was not possible to measure any reflectivity, due to extremely black colour of the samples. Furthermore, the photocatalytic activity strongly depends on the quantity of the exposed edge sites of $MoS_2$.[18] An increase in the $MoS_2$ nanosheet thickness leads to smoothing its surface, thus decreasing the area of the exposed edge sites of $MoS_2$.[53] This is due to the non-ideal growth mode, which takes place, when layered materials such as $MoS_2$, are synthesized by thermal ALD[53] and also by the very nature of $MoS_2$ formation. Indeed, the active edge sites of $MoS_2$ and their formation were identified theoretically[54] and experimentally[55] for both crystalline[56] and amorphous[57] $MoS_2$. These previous reports and results shown herein confirm that TNT layers + 2c $MoS_2$ (theoretically 2 S–Mo–S stacks) rendered the best photocatalytic performance in the liquid phase under both UV and VIS light irradiation, due to a higher amount of exposed edge sites compared to TNT layers + 1c $MoS_2$ and TNT layers + 5c $MoS_2$.

Gas phase photodegradation in Fig. 4 shows kinetics and the total hexane-to-$CO_2$ conversion achieved on the blank and
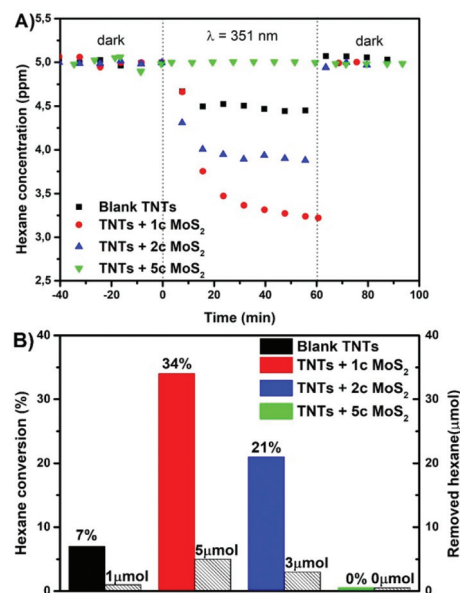


**Fig. 4** Gas phase photocatalysis: (A) changes in the hexane concentration in the reactor upon UV light irradiation, (B) conversion and removal of hexane for blank and $MoS_2$ decorated TNT layers. The "$Xc$" specifies the number of $MoS_2$ ALD cycles.

$MoS_2$ decorated TNT layers. The more detailed mechanism of hexane-to-$CO_2$ conversion is described in the ESI.† The highest photocatalytic conversion of hexane was achieved for 1 and 2 $MoS_2$ cycle decorated TNT layers with 34% and 21% conversion, removing the total of 5 μmol and 3 μmol of hexane which is ~5 and ~3 times higher compared to that of blank, respectively. The 5 $MoS_2$ cycle decoration of TNT layers did not show any measurable photoactivity.

By comparing Fig. 3 and 4, it is clear that the best photocatalytic activities in both the phases are obtained for different $MoS_2$ cycles (2c for the liquid and 1c for the gas phase). The reasons for this are not understood yet and require further investigation. However, while the difference in the homogeneity of the ALD $MoS_2$ nanosheets between the different nanotube layers used for the liquid and gas phase photocatalysis can be ruled out, the difference in the reactivity of the side edges of the $MoS_2$ nanosheets produced by 1c and 2c ALD cycles towards hexane degradation and diffusional and $MoS_2$ shading aspects of the different nanotube layers (with different morphological features) in general cannot be excluded.

## Conclusions

In conclusion, the homogeneous decoration of TNT layers with $MoS_2$ nanosheets using ALD was demonstrated in this work. The ALD $MoS_2$ decorated TNT layers possess enhanced photocurrent densities with improved charge carrier transport and increased photocatalytic activities, in both phases (liquid and gas). The presented results clearly show how promising is the

combination of 1D supports with 2D materials. These results may also pave the way for more sophisticated devices and applications of these nanomaterial classes in future.

## Conflicts of interest

There are no conflicts to declare.

## Acknowledgements

## Notes and references

1 J. M. Macak, M. Zlamal, J. Krysa and P. Schmuki, *Small*, 2007, **3**, 300–304.
2 M. Zlamal, J. M. Macak, P. Schmuki and J. Krýsa, *Electrochem. Commun.*, 2007, **9**, 2822–2826.
3 I. Paramasivam, H. Jha, N. Liu and P. Schmuki, *Small*, 2012, **8**, 3073–3103.
4 H. Sopha, M. Krbal, S. Ng, J. Prikryl, R. Zazpe, F. K. Yam and J. M. Macak, *Appl. Mater. Today*, 2017, **9**, 104–110.
5 D. Regonini, G. Chen, C. Leach and F. J. Clemens, *Electrochim. Acta*, 2016, **213**, 31–36.
6 N. R. De Tacconi, C. R. Chenthamarakshan, G. Yogeeswaran, A. Watcharenwong, R. S. De Zoysa, N. A. Basit and K. Rajeshwar, *J. Phys. Chem. C*, 2006, **110**, 25347–25355.
7 L. Tsui, T. Homma and G. Zangari, *J. Phys. Chem. C*, 2013, **117**, 6979–6989.
8 J. M. Macák, H. Tsuchiya, A. Ghicov and P. Schmuki, *Electrochem. Commun.*, 2005, **7**, 1133–1137.
9 K. Zhu, N. R. Neale, A. Alexander Miedaner and A. J. Frank, *Nano Lett.*, 2007, **7**, 69–74.
10 A. L. Linsebigler, G. Lu and J. T. Yates, *Chem. Rev.*, 1995, **95**, 735–758.
11 M. R. Hoffmann, S. T. Martin, W. Choi, D. W. Bahnemann and W. M. Keck, *Chem. Rev.*, 1995, **95**, 69–96.
12 K. Rajeshwar, *J. Appl. Electrochem.*, 1995, **25**, 1067–1082.
13 Z. Li, X. Meng and Z. Zhang, *J. Photochem. Photobiol., C*, 2018, **35**, 39–55.
14 J. Theerthagiri, R. A. Senthil, B. Senthilkumar, A. Reddy Polu, J. Madhavan and M. Ashokkumar, *J. Solid State Chem.*, 2017, **252**, 43–71.
15 R. G. Dickinson and L. Pauling, *J. Am. Chem. Soc.*, 1923, **45**, 1466–1471.
16 X. Zhou, M. Licklederer and P. Schmuki, *Electrochem. Commun.*, 2016, **73**, 33–37.
17 D. Dumcenco, D. Ovchinnikov, K. Marinov, P. Lazi, M. Gibertini, N. Marzari, O. Lopez Sanchez, Y.-C. Kung, D. Krasnozhon, M.-W. Chen, S. Bertolazzi, P. Gillet, A. Fontcuberta Morral, A. Radenovic and A. Kis, *ACS Nano*, 2015, **9**, 4611–4620.
18 Y.-J. Yuan, H.-W. Lu, Z.-T. Yu and Z.-G. Zou, *ChemSusChem*, 2015, **8**, 4113–4127.
19 W. Zhou, Z. Yin, Y. Du, X. Huang, Z. Zeng, Z. Fan, H. Liu, J. Wang and H. Zhang, *Small*, 2013, **9**, 140–147.
20 Z. Xiong, L. L. Zhang and X. S. Zhao, *Chem. – Eur. J.*, 2011, **17**, 2428–2434.
21 S.-M. Lam, J.-C. Sin, A. Z. Abdullah and A. R. Mohamed, *J. Mol. Catal. A: Chem.*, 2013, **370**, 123–131.
22 M. Sabarinathan, S. Harish, J. Archana, M. Navaneethan, H. Ikeda and Y. Hayakawa, *RSC Adv.*, 2017, **7**, 24754–24763.
23 M. Mehta, A. P. Singh, S. Kumar, S. Krishnamurthy, B. Wickman and S. Basu, *Vacuum*, 2018, **155**, 675–681.
24 W. Teng, Y. Wang, H. Huang, X. Li and Y. Tang, *Appl. Surf. Sci.*, 2017, **425**, 507–517.
25 M. Sun, Y. Wang, Y. Fang, S. Sun and Z. Yu, *J. Alloys Compd.*, 2016, **684**, 335–341.
26 Y. Yu, J. Wan, Z. Yang and Z. Hu, *J. Colloid Interface Sci.*, 2017, **502**, 100–111.
27 H. N. T. Phung, V. N. K. Tran, L. T. Nguyen, L. K. T. Phan, P. A. Duong and H. V. T. Le, *J. Nanomater.*, 2017, **2017**, 1–6.
28 Y. Yu, S.-Y. Huang, Y. Li, S. N. Steinmann, W. Yang and L. Cao, *Nano Lett.*, 2014, **14**, 553–558.
29 D. Voiry, M. Salehi, R. Silva, T. Fujita, M. Chen, T. Asefa, V. B. Shenoy, G. Eda and M. Chhowalla, *Nano Lett.*, 2013, **13**, 6222–6227.
30 E. Parzinger, B. Miller, B. Blaschke, J. A. Garrido, J. W. Ager, A. Holleitner and U. Wurstbauer, *ACS Nano*, 2015, **9**, 11302–11309.
31 C. Meng, Z. Liu, T. Zhang and J. Zhai, *Green Chem.*, 2015, **17**, 2764–2768.
32 D. Wang, Y. Xu, F. Sun, Q. Zhang, P. Wang and X. Wang, *Appl. Surf. Sci.*, 2016, **377**, 221–227.
33 F. Dvorak, R. Zazpe, M. Krbal, H. Sopha, J. Prikryl, S. Ng, L. Hromadko, F. Bures and J. M. Macak, *Appl. Mater. Today*, 2019, **14**, 1–20.
34 M. Krbal, J. Prikryl, R. Zazpe, H. Sopha and J. M. Macak, *Nanoscale*, 2017, **9**, 7755–7759.
35 D. Voiry, M. Salehi, R. Silva, T. Fujita, M. Chen, T. Asefa, V. B. Shenoy, G. Eda and M. Chhowalla, *Nano Lett.*, 2013, **13**, 6222–6227.
36 Y.-J. Yuan, Z.-J. Ye, H.-W. Lu, B. Hu, Y.-H. Li, D.-Q. Chen, J.-S. Zhong, Z.-T. Yu and Z.-G. Zou, *ACS Catal.*, 2016, **6**, 532–541.
37 J. Liang, C. Wang, P. Zhao, Y. Wang, L. Ma, G. Zhu, Y. Hu, Z. Lu, Z. Xu, T. Ma, T. Chen, Z. Tie, J. Liu and Z. Jin, *ACS Appl. Mater. Interfaces*, 2018, **10**, 6084–6089.
38 C. Liu, L. Wang, Y. Tang, S. Luo, Y. Liu, S. Zhang, Y. Zeng and Y. Xu, *Appl. Catal., B*, 2015, **164**, 1–9.
39 D. Wang, Y. Xu, F. Sun, Q. Zhang, P. Wang and X. Wang, *Appl. Surf. Sci.*, 2016, **377**, 221–227.
40 Y. Tian, Y. Song, M. Dou, J. Ji and F. Wang, *Appl. Surf. Sci.*, 2018, **433**, 197–205.
41 L. Yang, X. Zheng, M. Liu, S. Luo, Y. Luo and G. Li, *J. Hazard. Mater.*, 2017, **329**, 230–240.

42 L. Guo, Z. Yang, K. Marcus, Z. Li, B. Luo, L. Zhou, X. Wang, Y. Du and Y. Yang, *Energy Environ. Sci.*, 2018, **11**, 106–114.

43 H. Feng, N. Tang, S. Zhang, B. Liu and Q. Cai, *J. Colloid Interface Sci.*, 2017, **486**, 58–66.

44 L. Zheng, S. Han, H. Liu, P. Yu and X. Fang, *Small*, 2016, **12**, 1527–1536.

45 H. Sopha, A. Tesfaye, R. Zazpe, J. Michalicka, F. Dvorak, L. Hromadko, M. Krbal, J. Prikryl, T. Djenizian and J. M. Macak, *FlatChem*, 2019, **17**, 100130.

46 M. Motola, L. Satrapinskyy, T. Roch, J. Subrt, J. Kupcik, M. Klementova, M. Jakubickova, F. Peterka and G. Plesch, *Catal. Today*, 2017, **287**, 59–64.

47 H. Sopha, M. Baudys, M. Krbal, R. Zazpe, J. Prikryl, J. Krysa and J. M. Macak, *Electrochem. Commun.*, 2018, **97**, 91–95.

48 H. Li, Q. Zhang, C. C. R. Yap, B. K. Tay, T. H. T. Edwin, A. Olivier and D. Baillargeat, *Adv. Funct. Mater.*, 2012, **22**, 1385–1390.

49 L. Yang, C. Xie, J. Jin, R. Ali, C. Feng, P. Liu, B. Xiang, L. Yang, C. Xie, J. Jin, R. N. Ali, C. Feng, P. Liu and B. Xiang, *Nanomaterials*, 2018, **8**, 463.

50 A. Kuc, N. Zibouche and T. Heine, *Phys. Rev. B: Condens. Matter Mater. Phys.*, 2011, **83**, 245213.

51 Y.-J. Yuan, Z.-J. Ye, H.-W. Lu, B. Hu, Y.-H. Li, D.-Q. Chen, J.-S. Zhong, Z.-T. Yu and Z.-G. Zou, *ACS Catal.*, 2016, **6**, 532–541.

52 D. B. Nimbalkar, H.-H. Lo, P. V. R. K. Ramacharyulu and S.-C. Ke, *RSC Adv.*, 2016, **6**, 31661–31667.

53 T. A. Ho, C. Bae, S. Lee, M. Kim, J. M. Montero-Moreno, J. H. Park and H. Shin, *Chem. Mater.*, 2017, **29**, 7604–7614.

54 B. Hinnemann, P. G. Moses, J. Bonde, K. P. Jørgensen, J. H. Nielsen, S. Horch, A. I. Chorkendorff and J. K. Nørskov, *J. Am. Chem. Soc.*, 2005, **127**, 5308–5309.

55 T. F. Jaramillo, K. P. Jørgensen, J. Bonde, J. H. Nielsen, S. Horch and I. Chorkendorff, *Science*, 2007, **317**, 100–102.

56 J. Bonde, P. G. Moses, T. F. Jaramillo, J. K. Nørskov and I. Chorkendorff, *Faraday Discuss.*, 2009, **140**, 219–231.

57 C. G. Morales-Guio and X. Hu, *Acc. Chem. Res.*, 2014, **47**, 2671–2681.